The lower exosphere of Titan: Energetic neutral atoms absorption and imaging

P. Garnier, I. Dandouras, D. Toublanc, E. C. Roelof, P. C. Brandt, D. G. Mitchell, S. M. Krimigis, N. Krupp, D. C. Hamilton, Odile Dutuit, et al.

The lower exosphere of Titan: Energetic neutral atoms absorption and imaging

P. Garnier,[1,2] I. Dandouras,[1] D. Toublanc,[1] E. C. Roelof,[3] P. C. Brandt,[3] D. G. Mitchell,[3] S. M. Krimigis,[3] N. Krupp,[4] D. C. Hamilton,[5] O. Dutuit,[6] and J.-E. Wahlund[2]

Received 8 January 2008; revised 17 April 2008; accepted 24 June 2008; published 30 October 2008.

[1] The Saturn magnetosphere interacts with the Titan atmosphere through various mechanisms. One of them leads, by charge exchange reactions between the energetic Saturnian ions and the exospheric neutrals of Titan, to the production of energetic neutral atoms (ENAs). The Ion and Neutral Camera (INCA), one of the three sensors that comprise the Magnetosphere Imaging Instrument (MIMI) on the Cassini/Huygens mission to Saturn and Titan, images the ENA emissions in the Saturnian magnetosphere. This study focuses on the ENA imaging of Titan (for 20–50 keV H ENAs), with the example of the Ta Titan flyby (26 October 2004): our objective is to understand the positioning of the ENA halo observed around Titan. Thus we investigate the main ENA loss mechanisms, such as the finite gyroradii effects for the parent ions, or the charge stripping with exospheric neutrals. We show that multiple stripping and charge exchange reactions have to be taken into account to understand the ENA dynamics. The use of an analytical approach, taking into account these reactions, combined with a reprocessing of the INCA data, allows us to reproduce the ENA images of the Ta flyby and indicates a lower limit for ENA emission around the exobase. However, the dynamics of energetic particles through the Titan atmosphere remains complex, with an inconsistency between the ENA imaging at low and high altitudes.

Citation: Garnier, P., et al. (2008), The lower exosphere of Titan: Energetic neutral atoms absorption and imaging, *J. Geophys. Res.*, *113*, A10216, doi:10.1029/2008JA013029.

1. Introduction

[2] The Cassini mission has substantially progressed our knowledge of the Saturnian environment, since the Saturn Orbit Insertion in July 2004. Titan, the largest among the Saturnian satellites, is one of the main objectives of the mission. Its dense nitrogen atmosphere, which is not protected by an intrinsic magnetic field, interacts directly with the Saturnian magnetosphere, through various phenomena [*Brecht et al.*, 2000; *Kallio et al.*, 2004].

[3] In particular, the energetic ions of the Saturnian magnetosphere may undergo charge exchange reactions with the Titan cold exospheric neutrals, producing energetic neutral atoms (ENAs). These can then be detected like photons, by ENA imagers, such as the INCA instrument (Ion and Neutral Camera) onboard Cassini. This detector, which is part of the MIMI experiment [*Krimigis et al.*, 2004], comprising also two other energetic particle instruments (CHEMS for Charge Energy Mass Spectrometer, and LEMMS or Low Energy Magnetospheric Measurement System), gives the ENA flux integrated along the lines of sight inside the instrument field of view ($90 \times 120°$). These ENA images allow to infer information on both the neutral and ion populations [*Roelof*, 1987], in particular in the upper part of the Titan atmosphere, where the neutral densities cannot be measured directly (the INMS instrument gives neutral densities up to 2000 km altitude only [*Waite et al.*, 2005]).

[4] The ENA emissions due to the Titan exosphere can even be used to infer exospheric distributions up to 40,000 km altitude (Brandt, private communication). The Titan exosphere is indeed very extended, with mostly satellite particles in its outer part: the Hill radius [*Hill*, 1878] for Titan, which gives the limit of its gravitational influence and thus a good estimate for the external limit of its exosphere, is around 50,000 km.

[5] The interaction between the Titan exosphere and the Saturnian magnetosphere was already analyzed, before the arrival of Cassini at Saturn [*Amsif et al.*, 1997; *Dandouras and Amsif*, 1999]. The importance of the limb brightening effect and the finite parent ion gyroradii effects were later confirmed by the first Cassini data [*Mitchell et al.*, 2005],

[1]Centre d'Etude Spatiale des Rayonnements, CNRS/Paul Sabatier University, Toulouse, France.
[2]Swedish Institute of Space Physics, Uppsala, Sweden.
[3]Applied Physics Laboratory, Johns Hopkins University, Laurel, Maryland, USA.
[4]Max-Planck-Institut fur Sonnensystemforschung, Lindau, Germany.
[5]Department of Physics, University of Maryland, College Park, Maryland, USA.
[6]Laboratoire de Planetologie de Grenoble, Universite Joseph Fourier, Grenoble, France.

0148-0227/08/2008JA013029

for the Ta and Tb Titan flybys (respectively 26 October and 13 December 2004). A first analysis of the Ta INCA data resulted in a new exosphere model based on the Cassini results [*Garnier et al.*, 2007a].

[6] *Garnier et al.* [2007a] study pinpointed to the issue of ENA dynamics in the Titan atmosphere (for H ENAs with 20–50 keV energy range), which determines the position of the ENA halo (maximum ENA flux measured) around Titan. The limit for the ENA emission inducing this halo can be caused, first, by mechanisms preventing the parent ions from entering certain atmospheric regions, such as the finite gyroradii effects (here in the case of more realistic trajectories than just circular ones as in the previous studies). Then, loss mechanisms must play a role, through a thermalization or through a change of the charge state for the particles (an ENA ionized cannot be detected as an ion by the ENA imager): we present here a statistical analysis of the number of collisions, based on the calculation of the optical thickness.

[7] The first sections of our study will thus analyze the following processes:

[8] 1. $H^+ \rightarrow H$ Process no. 1: ENA formation, taking into account finite gyroradii effects (analyzed in section 2);

[9] 2. $H \rightarrow H^+$ Process no. 2: ENA ionization (analyzed in section 3);

[10] 3. $H^+ \rightarrow H$ Process no. 3: Reneutralization of ionized ENA (analyzed in section 4).

[11] Finally, we will compare the reprocessed INCA data, for the Ta flyby, with ENA flux simulations (with both analytical and numerical approaches), and conclude on the complex dynamics of ENAs through the Titan atmosphere.

2. Parent Ion Finite Gyroradii Effects

[12] The energy range of the INCA sensor (above 10 keV), combined with the relatively low Saturn magnetic field value in the Titan environment, lead to very important gyroradii effects for the ENA parent ions. Thus protons with energies between 20 and 50 keV, for a 5-nT magnetic field (a value consistent with both Voyager and Cassini data [*Neubauer et al.*, 2006]), will have gyroradii between 4084 km and 6457 km, which are comparable or even larger than the Titan radius (2575 km). As a consequence, Titan will prevent the presence of such ions in certain regions, due to the shadow induced by these gyroradii effects.

[13] These effects were previously studied by *Dandouras and Amsif* [1999] for circular trajectories. However, the plasma corotation in the Saturnian magnetosphere implies that the ion trajectories should be rather cycloidal than just circular. Such trajectories could significantly change the importance of these gyroradii effects.

2.1. Cycloidal Trajectories

[14] In order to introduce the corotation influence, we developed simple equations of such cycloidal trajectories, by combining a gyration and a translation (with velocity v_c). This formalism will be used in this study of the finite gyroradii effects and also in section 4. to simulate the ion trajectories more realistically than with just circular trajectories. The flow velocity v_c was taken, for this analysis, at 120 km/s, which is consistent with both Voyager and Cassini data for the Titan environment (at about 20 Saturn radii far from Saturn): *Sittler et al.* [2005] found a velocity range of 80–150 km/s for the Voyager 1 flyby; *Hartle et al.* [2006a, 2006b] found a flow velocity between 90 and 130 km/s for Cassini CAPS data, and *Szego et al.* [2005] inferred a corotation velocity around 120–160 km/s for Cassini CAPS measurements. Moreover, the flow velocity has to be taken in the Cassini reference frame. However, the velocities of Cassini in the Titan frame and of Titan in a Sun-linked Saturn frame are both of the same order, about 5 km/s, which is negligible in our case, compared with both the flow velocity measured and the uncertainties on its value. We may also add that the drift induced by the magnetic field gradient is not important in this environment.

[15] The following formulas, used to simulate proton trajectories for an energy E and a constant pitch angle, are issued from the gyration equation (in a constant magnetic field frame), transformed to the frame of reference of Titan. We assume this one to be the same as a Cassini frame centered on Titan as explained above, through a translation with velocity v_c. The coordinate axis used here, $\overrightarrow{X}$, $\overrightarrow{Z}$ and $\overrightarrow{Y}$, correspond respectively to the corotation velocity direction $\overrightarrow{v_c}$ (which is here supposed to be perpendicular to the magnetic field), the opposite direction of the magnetic field $\overrightarrow{-B}$ and finally $\overrightarrow{Y}$ completes the right-handed system.

$$\begin{cases} X(t) = -A * \sin(\omega * t + \phi) - \dfrac{V_{Y_0}}{\omega} + v_c * t + X_0 \\ Y(t) = A * \cos(\omega * t + \phi) + \dfrac{V_{X_0}}{\omega} + Y_0 \\ Z(t) = V_{Z_0} * t + Z_0 \end{cases} \tag{1}$$

[16] The gyration angular velocity ω is defined by $\omega = \frac{qB}{m}$ (q and m are the ion electric charge and mass); A and ϕ are given by the following system:

$$\begin{cases} A * \sin(\phi) + \dfrac{V_{Y_0}}{\omega} = 0 \\ A * \cos(\phi) + \dfrac{V_{X_0}}{\omega} = 0. \end{cases} \tag{2}$$

which leads to (with the sign depending on those of V_{X0} and V_{Y0}):

$$\begin{cases} A = \pm \dfrac{1}{\omega} * \sqrt{V_{X_0}^2 + V_{X_0}^2} \\ \phi = \arctan\left(\dfrac{V_{Y_0}}{V_{X_0}}\right). \end{cases} \tag{3}$$

(X_0, Y_0, Z_0) are the initial position coordinates in the Cassini frame, and (V_{X0}, V_{Y0}, V_{Z0}) are the initial velocity coordinates in the corotating plasma frame. However, the ion energies in our study are such (>20 keV) that the corotation energy can be neglected: there is a factor 1000 in energy between a 50 keV ion and a particle moving at 100 km/s. Thus we will later talk about a unique energy E for the ions.

[17] The simulation of such cycloidal trajectories leads to circular-like trajectories, with a global movement toward the positive X axis. For energies between 20 and 50 keV, an ion will move, after one gyration period, about 1500 km (to be compared with the gyroradii of about 4000–6500 km) for v_c = 120 km/s.

2.2. Shadow Effects for ENA Parent Ions

[18] The purpose is to perform a similar study as done by *Dandouras and Amsif* [1999; see Figure 6], but in this case for more realistic trajectories than simple circular ones, by using the formalism developed above. The mechanism discussed here is the creation of a shadow region, where the trajectories of the energetic ions are such that they cannot lead to ENAs later detected by the INCA imager (without the parent ions being previously absorbed in the atmosphere).

[19] We assume a constant pitch angle of $\pi/2$, which induces ion trajectories in the plane defined by the Cassini position along the Z axis. This assumption leads to maximum apparent gyroradii, and thus to a maximum shadow induced for the parent ions. We may add that the results obtained by *Krimigis et al.* [1981], with the Voyager data, globally indicated ion pitch angle distributions peaked around $\pi/2$. However, the recent analysis of the LEMMS data [*Garnier et al.*, 2007b] shows quasi-isotropic distributions for the energetic protons.

[20] Note that the magnetic field configuration is here considered as homogeneous, and the draping effects around Titan are ignored. Even if these effects are obviously real, they do not influence significantly the energetic ion trajectories at the scale of a gyration [*Garnier et al.*, 2007b]: the characteristic thickness of the interaction layer, where the magnetic field draping develops around the Titan ionosphere [see *Backes et al.*, 2005], is negligible compared to the gyroradii of the ions considered. Thus as a first approach, such a configuration can lead to a correct estimation of the finite gyroradii effects for the parent ions.

[21] The principle is to find the conditions, with the formalism introduced before, which allow an ion to get tangent to the exobase (taken as the lower limit, below which an ion is here considered as lost; this assumption will be discussed later in this paper) at a moment t_1 and then to collide with a neutral at a time t_2 with such a trajectory that it can reach the imager later, without getting below the exobase at any moment. This principle allows to find the limit condition for a given line of sight, and then, by testing all possible lines of sight, to draw the curve delimiting the shadow induced for the ions by these gyroradii effects.

[22] The mathematical transcription of the conditions described above leads to a system of nonlinear equations. We can then infer the expressions for t_1 and t_2, which lead to the limit of the shadow for ENA parent ions.

[23] An example of result is shown in Figure 1, with an energy of about 50 keV and a position of the satellite defined by $[X_{sat}, Y_{sat}, Z_{sat}] = [8000\text{ km} + R_T, 0, 0]$ (with the Titan radius $R_T = 2575$ km). This configuration shows the importance of the shadow induced for the ions, which extends until 5.5 R_T downstream Titan. Globally, the shadow is very similar to the one obtained for circular trajectories, even if it is more extended with cycloidal trajectories (about 0.5 R_T more on the X axis). We get the same asymmetry ''left/right'' which is expected for any satellite configuration and any type of ion trajectory [see *Dandouras and Amsif*, 1999].

[24] By testing several satellite positions (in the X-Y plane, and also on the Z axis), as well as various energies or corotation velocities, we can make the following conclusions. First, the shadow systematically keeps the asymmetry ''left/right.'' Second, the importance of these gyroradii effects increases with energy (since the gyroradii increase in the same time), decreases with Z_{sat} (since the apparent exobase in the X-Y plane is maximum at $Z_{sat} = 0$ and then decreases), but can either decrease or increase by increasing the corotation velocity: it increases for vantage points along the positive Y axis, but decreases for vantage points along the negative Y axis (the gyroradii effects are here flattened by a high v_c). When the vantage point is too close to Titan the shadow effect becomes complicated (this the case in Figure 1): the frontier of the shadow region intersects the imager position, as soon as the distance between Cassini and Titan is too small to allow the ion to move freely between them. Such a situation thus appears for a distance smaller than the ion gyration diameter.

[25] The use of cycloidal trajectories instead of circular ones does not change the qualitative influence on the parent ion finite gyroradii effects, but it can change quantitatively and introduce asymmetries in these effects, depending on the configuration taken.

[26] Moreover, we can show that, in some cases, such ions (with cycloidal trajectories) can pass through Titan, even with a 90° pitch angle and without crossing the exobase. This can be the case in particular away from the equator, with an apparent exobase (in planes parallel to the equator) which decreases. A rough estimation leads to the Z limit for observing such trajectories (for 90° pitch angle protons): $Z > Z_{lim} = \sqrt{H_c^2 - (Vc * 2\pi/w)^2/4} \approx R_T/2$ for $B = 5$ nT and an exobase at $H_c = 1425$ km (as indicated by INMS for Ta [see *Waite et al.*, 2005]).

[27] The imaging of the Titan environment, with using the INCA data, can show these gyroradii effects (see *Garnier et al.* [2007a], for the Ta flyby). In addition, we can confirm, as indicated in *Garnier et al.* [2007a], that the shadow induced for the parent ions cannot imply a specific loss of ENAs in the ''right'' part of the Titan Ta flyby image discussed in our previous paper (the part with the bright ENA semicrescent). However, we don't expect the images to follow exactly the shadow effects simulated here: some differences may be introduced by the draping of the magnetic field around Titan (but which occurs in scales shorter than the ion gyroradii discussed here), by the pitch angle distribution more complex than considered above, and by the plasma corotation, whose velocity and direction are dynamic.

[28] Moreover, these gyroradii effects assume a hard limit at the exobase, but where does this limit come from? We will now discuss this point, by analyzing the ENA loss mechanisms (by ionization) leading to this hard limit, in order to understand the position of the ENA halo around Titan.

3. Absorption of H ENAs by Ionization

[29] The ionization is a second mechanism which can imply a loss of ENAs, after the shadow effect induced for the parent ions by the finite gyroradii effects (and described above).

[30] The ENAs (hydrogen atoms in our case) can be ionized through various mechanisms:

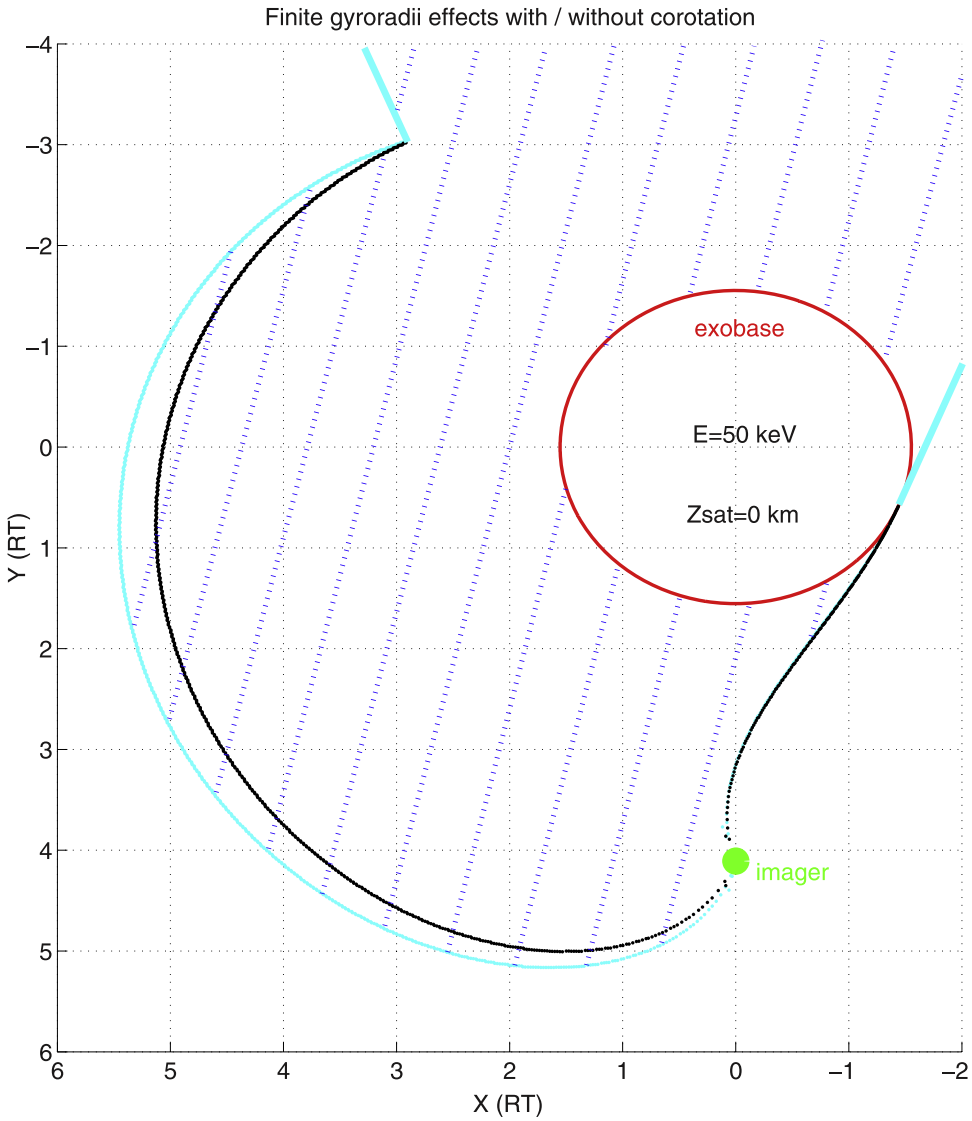

Figure 1. Finite gyroradii effects in the *X*-*Y* plane (units: Titan radii R_T) for 90° pitch angle protons, with B = [0, 0, −5 nT] and 50 keV energy. The green square determines the imager position, and the blue/black lines show the shadow limits for corotation velocities respectively. v_c = [120 km/s, 0, 0] and v_c = 0 km/s (circular trajectories). The blue dots area shows the shadow induced for the ENA parent ions with cycloidal trajectories: no ENA can be produced inside this area and then detected by the imager.

[31] 1. $H_{ENA} + e^- \rightarrow H^+ + 2e^-$: electron ($e^-$) impact ionization.

[32] 2. $H_{ENA} + h\nu \rightarrow H^{+n} + ne^-$: ionization by photons ($h\nu$).

[33] 3. $H_{ENA} + X^+ \rightarrow H^+ + X$: charge stripping with an ion X^+.

[34] 4. $H_{ENA} + X \rightarrow H^+ + all$: charge stripping with a neutral X.

[35] The three first mechanisms will not be discussed in detail, since they are negligible compared to the charge stripping reactions with the Titan atmospheric neutrals.

[36] Concerning the electron impact ionization, which could occur either with ionospheric or magnetospheric electrons, the electron densities (see *Neubauer et al.* [1984] for magnetospheric electrons with Voyager data and *Wahlund et al.* [2005], for ionospheric electrons with the Cassini RPWS data) are smaller than the neutral Titan atmospheric densities, and the cross-sections (see NIST online database) are also smaller than for charge stripping. The photoionization cannot ionize ENAs, since the photon density near Titan (calculated by $n_{photons} = \frac{F}{c}$ with the unattenuated solar flux F at Saturn and the celerity c) is really negligible, and the photoabsorption cross-sections [see *Schunk and Nagy*, 2000] are smaller than those for charge stripping.

[37] The charge stripping collisions with ions have also a much smaller influence than the charge stripping with neutrals. If the cross-sections are very similar [*McClure*, 1966; *Phaneuf et al.*, 1978], the ion densities (for ionospheric ions with *Toublanc et al.* [1995] and magnetospheric ions with *Krimigis et al.* [1983]) are again much smaller than the neutral densities.

Table 1. Charge Stripping Cross-Sections σ_i (cm^2) Between H ENAs With Energy E (keV) and Atmospheric Neutral Species i[a]

E	σ_1 (fit 1/2)	σ_2 (fit 1/2)	σ_3 (fit 1/2)	σ_4	σ_5
10	$6.1/8.2 \times 10^{-17}$	$2.8/1.7 \times 10^{-16}$	$2.4/1.7 \times 10^{-16}$	1.6×10^{-16}	5.9×10^{-17}
20	$7/11.5 \times 10^{-17}$	$3.9/2.9 \times 10^{-16}$	$3.2/2.1 \times 10^{-16}$	2×10^{-16}	7.5×10^{-17}
30	$7.1/13.7 \times 10^{-17}$	$4.6/4.2 \times 10^{-16}$	$3.6/2.3 \times 10^{-16}$	2.2×10^{-16}	8×10^{-17}
40	$7/14.9 \times 10^{-17}$	$4.9/5.2 \times 10^{-16}$	$3.7/2.4 \times 10^{-16}$	2.3×10^{-16}	8.1×10^{-17}
50	$6.7/15.2 \times 10^{-17}$	$5.1/5.9 \times 10^{-16}$	$3.8/2.4 \times 10^{-16}$	2.3×10^{-16}	8.1×10^{-17}
60	$6.4/14.9 \times 10^{-17}$	$5/6.3 \times 10^{-16}$	$3.7/2.4 \times 10^{-16}$	2.4×10^{-16}	8×10^{-17}
70	$6.1/14.1 \times 10^{-17}$	$4.9/6.5 \times 10^{-16}$	$3.7/2.4 \times 10^{-16}$	2.4×10^{-16}	7.7×10^{-17}
80	$5.7/13.1 \times 10^{-17}$	$4.7/6.5 \times 10^{-16}$	$3.6/2.3 \times 10^{-16}$	2.3×10^{-16}	7.1×10^{-17}
90	$5.4/11.9 \times 10^{-17}$	$4.5/6.3 \times 10^{-16}$	$3.5/2.3 \times 10^{-16}$	2.2×10^{-16}	6.5×10^{-17}
100	$5.2/10.8 \times 10^{-17}$	$4.2/6 \times 10^{-16}$	$3.5/2.2 \times 10^{-16}$	2.1×10^{-16}	5.8×10^{-17}

[a](1) $H + H_2 \xrightarrow{\sigma_1} H^+ + all$: *Toburen et al.* [1968], Hsieh (private communication, 2005), with two different fits (fit 1/2). (2) $H + CH_4 \xrightarrow{\sigma_2} H^+ + all$: *Eliot* [1977], Hsieh (private communication, 2005), with two different fits (fit 1/2). (3) $H + N_2 \xrightarrow{\sigma_3} H^+ + all$: *Toburen et al.* [1968], Hsieh (private communication, 2005), with two different fits (fit 1/2). (4) $H + N \xrightarrow{\sigma_4} H^+ + all$: *Barnett and Reynolds* [1958]. (5) $H + H \xrightarrow{\sigma_5} H^+ + all$: *Barnett and Reynolds* [1958].

3.1. Ionization Probability: Optical Thickness Definition

[38] Our purpose in this section is to estimate the probability for an ENA to be ionized in the Titan atmosphere. We can thus better understand the loss mechanisms for ENAs, and determine the lower limit for their emission.

[39] Instead of developing a full ENAs absorption model, we will here use a simple analysis, by calculating the optical thickness τ for ENAs for this mechanism.

[40] The optical thickness gives the statistical number of collisions cumulated along a trajectory Γ_p, by integrating the inverse of the mean free path λ along the trajectory:

$$\tau(p,E) = \int_{\Gamma_p} \frac{ds}{\lambda(s,E)} = \int_{\Gamma_p} (n(s) * \sigma(E))ds \qquad (4)$$

[41] The optical thickness is calculated for a trajectory defined by the imager position, an impact parameter p and for an energy E (corresponding to the relative velocity between the H ENA and the particle colliding with it). σ (in cm^2) is the cross-section for the collision studied at the energy E, and n gives the density (in cm^{-3}) of the particles with which the H ENA collides at the local point of integration.

3.2. Charge Stripping of H ENAs on Neutrals

[42] The main ionization mechanism which can concern the ENAs is the charge stripping collisions of these ENAs on the exospheric neutrals of Titan.

[43] The neutral densities used to calculate the optical thickness with equation (4) come from our exosphere model [*Garnier et al.*, 2007a], which is consistent with both the INMS data for the first Titan flyby Ta [*Waite et al.*, 2005] and the Vervack model [*Vervack et al.*, 2004]. The densities below the exobase are taken from the D. Toublanc atmospheric model [adapted from *Toublanc et al.*, 1995]. We use the five main neutral species at the exobase: N_2, CH_4, H_2, H and N ($4S$).

[44] The charge stripping cross-sections needed for this study (for energies of 20–50 keV) come from several references depending on the species concerned, and are given in Table 1.

[45] Figure 2 gives the optical thickness profile, for a 50 keV H ENA coming from the infinite, and for impact parameters p from 800 km altitude up to 15000 km altitude. The imager is positioned at 8000 km altitude (altitude of Cassini for the INCA image studied in *Garnier et al.* [2007a]). The statistical number of collisions, for each H ENA, with exospheric neutrals, decreases from 4000 at p = 800 km altitude, to about 10^{-3} at p = 15,000 km altitude. The limit between the optically thick and the optically thin parts of the atmosphere (where there is statistically one collision, τ = 1) is here at $p \approx 1525$ km, just above the exobase (H_c = 1425 km).

[46] The limit where τ = 1 varies between about 1500 and 1550 km, depending on the energy considered (from 20 to 50 keV) and on the reference used for the cross-section values. In addition, the optical thickness decreases from 10 to 0.1 between about p = 1300 and 1850 km altitude.

[47] The charge stripping reactions between H ENAs and exospheric neutrals is the main loss for ENAs in the Titan atmosphere. However, an H ENA undergoes statistically at least one collision only below p = 1550 km, so that we cannot put an emission cut-off at altitudes of 1800–1900 km, as proposed in our previous paper [*Garnier et al.*, 2007a]. The numerical emission cut-off should be indeed around or below p = 1550 km altitude: around if an ENA once ionized is really lost for ENA imaging, below if such ENAs ionized can be neutralized again. Thus we will now study the possibility for ENAs ionized to become again ENAs and then be detected by the instrument.

4. Reneutralization of Ionized H ENAs

[48] We analyzed, in the previous section, the various ionization mechanisms which H ENAs may undergo in the Titan atmosphere. The charge stripping reactions on exospheric neutrals seem to be able to ionize these ENAs under an impact parameter around 1550 km altitude. However, are these ENAs completely lost for imaging?

[49] We will now do a similar study, as previously on the ionization mechanisms, on the reneutralization of newly ionized ENAs, through charge exchange with exospheric neutrals (which is the only mechanism able to transform the ions in ENAs). We will thus calculate the number of neutralizations of these ions, by calculating the optical thickness τ of H^+ (with the energy of the ENAs studied, 20–50 keV) for charge exchange with neutrals, not along a

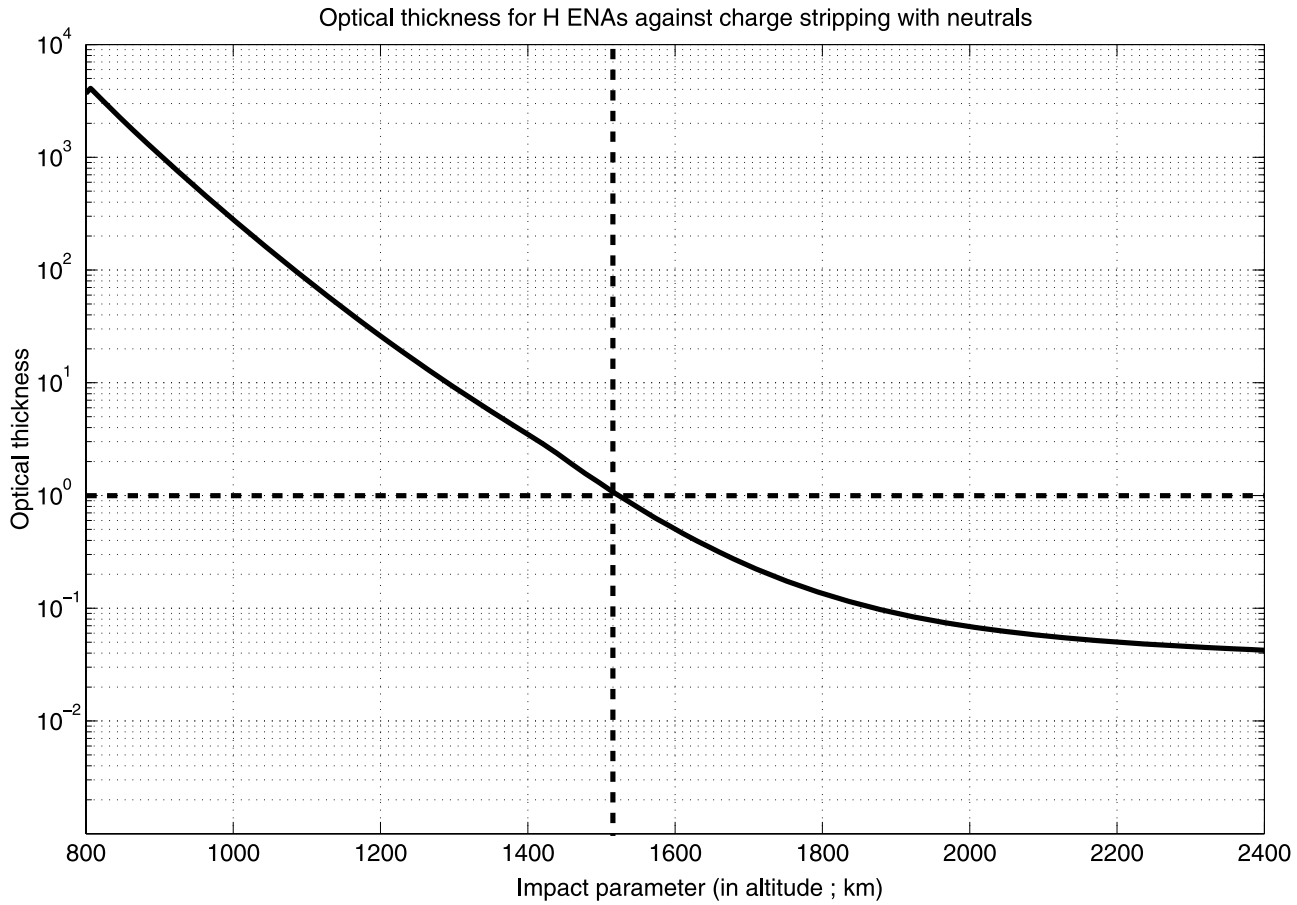

Figure 2. Optical thickness for 50 keV H ENAs, for charge stripping with exospheric neutrals (process no. 2). The dashed lines place the limit where the ENAs undergo statistically one collision.

line of sight, but along the ion trajectory Γ_p from the ionization point:

$$\tau(p,E) = \int_{\Gamma_p} \frac{ds}{\lambda(s,E)} = \sum_k \int_{\Gamma_p} (n_k(s) * \sigma_k(E)) \frac{ds}{dt} * dt \quad (5)$$

with:

$$s(t) = \int_{t_0}^{t} \sqrt{V_x^2(q) + V_y^2(q)} dq \quad (6)$$

where p is the impact parameter of the line of sight, E is the ENA energy, n_k gives the density (cm^{-3}) of the neutral species k, σ_k is the charge exchange cross-section between H^+ and the neutral species k, and V_x/V_y are the ion velocity components (in the equatorial plane *X*-*Y*, see below for the frame definition).

[50] Figure 3 shows a schematic view of our simulations, with the cycloidal trajectories for the newly ionized H ENAs (with the formalism and the parameters defined previously in section 2.1). We consider a line of sight of the imager, defined by an impact parameter p (p = 3500 km altitude on the figure). We consider that a 20 keV H ENA, whose direction is along the line of sight and toward the imager, is actually ionized at the point shown, taken as the closest point from Titan within this line of sight. This corresponds to a maximum condition also for the neutralization probability. The ion trajectory is cycloidal, and the ion gets closer to Titan after each period (this is due to the configuration taken for the imager position and the line of sight chosen), until it virtually crosses the Titan surface. The part of the trajectory before the ionization point is also virtual: it is necessary in our numerical simulations, as an initial point for the ion (we use constraints on the initial velocities values V_x and V_y, but it has no physical role). The (*X*, *Y*, *Z*) frame used for this study is the one described in section 2.1. In addition, we consider here only trajectories in the X-Y plane (thus with 90° pitch angle protons, and Z_{Imager} = 0 km).

[51] The neutral densities used in equation (5) come again from our exosphere model [*Garnier et al.*, 2007a]. The cross-sections needed are issued from several references, depending on the species concerned, and are given in Table 2.

[52] The principle is to calculate the optical thickness (with equation (5)) of new ions (former H ENAs), along their cycloidal trajectory and from the ionization point, for charge exchange with the atmospheric neutrals. For an imager position, we take a range of impact parameters p.

[53] The result depends highly on the configuration taken. The probability for the ion to be neutralized increases essentially at each period around the closest point from Titan (where the densities are maximum). Thus for the

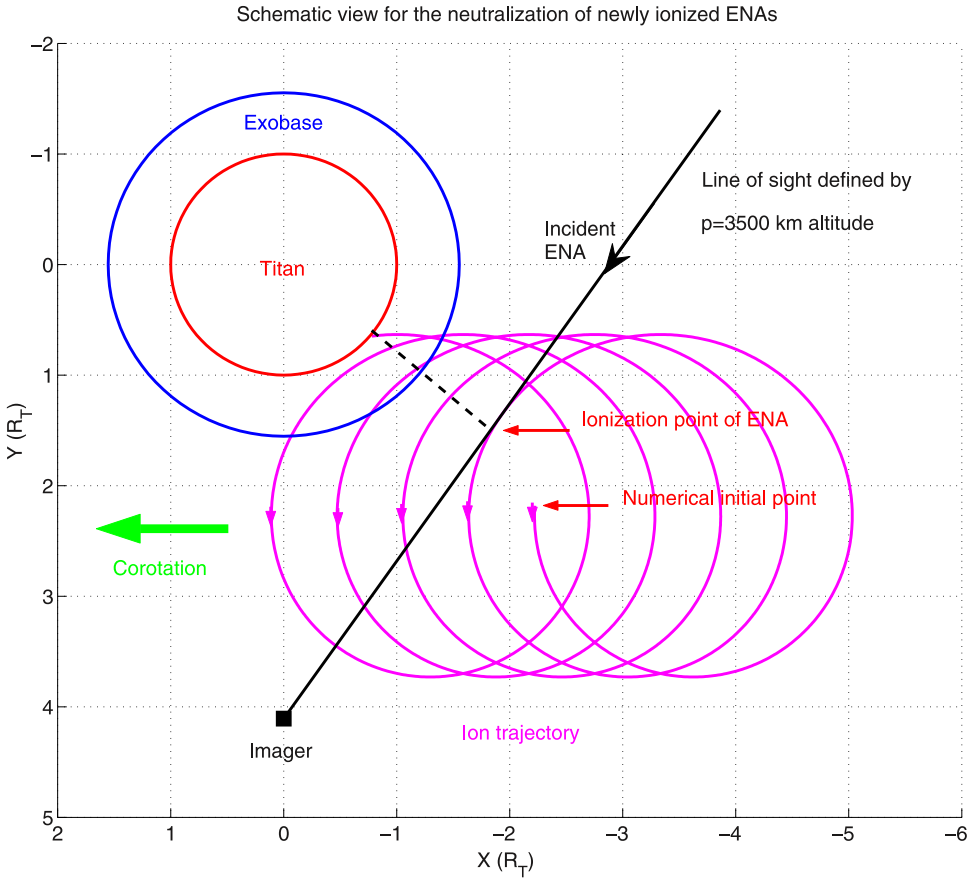

Figure 3. Principle for the analysis of the neutralization of newly ionized ENAs (process no. 3). We consider first a 20-keV incident H ENA, coming along a defined line of sight. Then the ENA is ionized by charge exchange at the "ionization point," before the new ion follows a cycloid motion, along which it may be neutralized again by charge exchange collisions. The cycloid motion before the "ionization point" is not physical and only due to the numerical simulation details.

configuration shown in Figure 3, the number of collisions will increase more and more rapidly after each gyration, until the trajectory virtually crosses the Titan surface; but for a line of sight defined so that the ion gets further and further from Titan after each period, the number of collisions will also increase, but less and less rapidly (since the neutral densities decrease with altitude).

[54] In particular, we estimate when the newly ionized ENA will be statistically reneutralized, i.e., when $\tau = 1$. Figure 4 shows such an analysis, for a configuration similar

Table 2. Charge Exchange Cross-Sections σ_i (cm^2) Between Protons With Energy E (keV) and Atmospheric Neutral Species i[a]

E	σ_1	σ_2	σ_3	σ_4	σ_5
10	1.1×10^{-15}	1.6×10^{-15}	8.3×10^{-16}	5.2×10^{-16}	7.3×10^{-16}
20	7.3×10^{-16}	1.3×10^{-15}	6.1×10^{-16}	3.8×10^{-16}	4×10^{-16}
30	5.5×10^{-16}	9.3×10^{-16}	4.1×10^{-16}	2.8×10^{-16}	2.5×10^{-16}
40	4.3×10^{-16}	6.7×10^{-16}	2.7×10^{-16}	2×10^{-16}	1.6×10^{-16}
50	3.4×10^{-16}	4.9×10^{-16}	1.8×10^{-16}	1.5×10^{-16}	9×10^{-17}
60	2.7×10^{-16}	3.6×10^{-16}	1.2×10^{-16}	1.2×10^{-16}	6×10^{-17}
70	2.2×10^{-16}	2.7×10^{-16}	9×10^{-17}	9×10^{-17}	4×10^{-17}
80	1.8×10^{-16}	2×10^{-16}	6×10^{-17}	7×10^{-17}	3×10^{-17}
90	1.4×10^{-16}	1.5×10^{-16}	4×10^{-17}	6×10^{-17}	2×10^{-17}
100	1.2×10^{-16}	1.2×10^{-16}	3×10^{-17}	4×10^{-17}	1×10^{-17}

[a](1) $H^+ + N_2 \xrightarrow{\sigma_1} H + N_2^+$: *Toburen et al.* [1968], *Eliot* [1977] and Hsieh (private communication, 2005). (2) $H^+ + CH_4 \xrightarrow{\sigma_2} H + CH_4^+$: *Toburen et al.* [1968], *Eliot* [1977] and Hsieh (private communication, 2005). (3) $H^+ + H_2 \xrightarrow{\sigma_3} H + H_2^+$: *Eliot* [1977], *Rudd et al.* [1983], Hsieh (private communication, 2005). (4) $H^+ + N \xrightarrow{\sigma_4} H + N^+$: *Barnett and Reynolds* [1958]. (5) $H^+ + H \xrightarrow{\sigma_5} H + H^+$: *McClure* [1966].

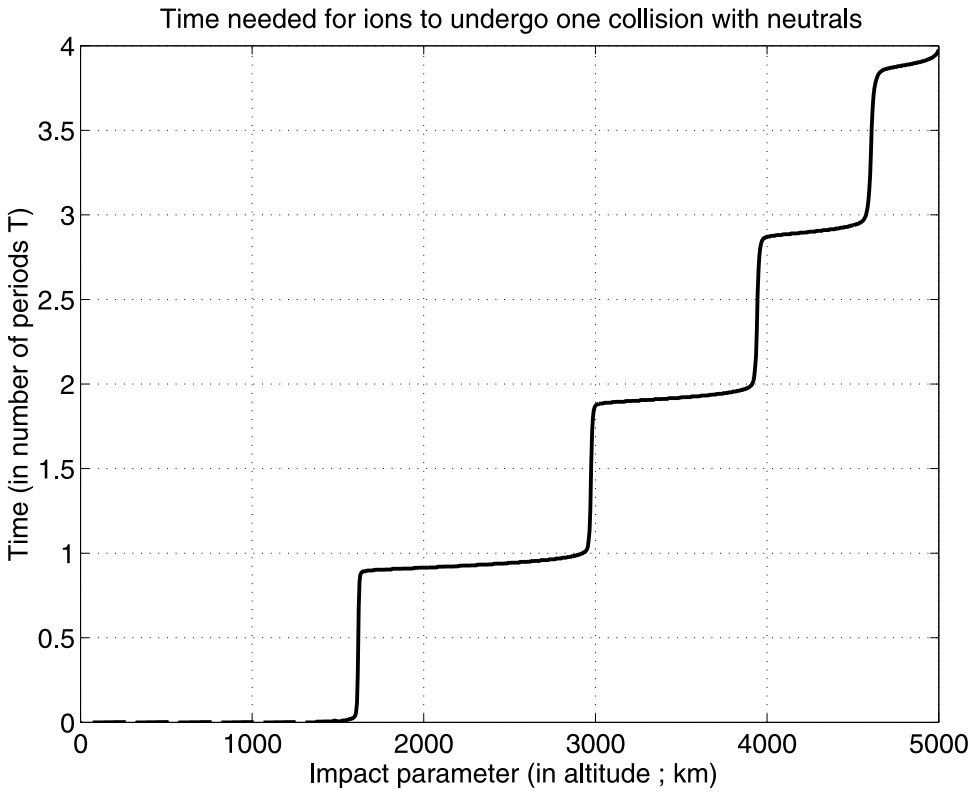

Figure 4. Time, in number of gyration periods T, needed for a 20-keV ENA ionized (at the closest point from Titan along the line of sight defined by the impact parameter p) to statistically undergo one collision with the atmospheric neutrals (process no. 3).

to that of Figure 3. We give here the time, in number of gyration periods T ($T = \frac{2\pi}{\omega}$ with ω being the gyro angular frequency $w = \frac{qB}{m}$), necessary for a proton to be neutralized by charge exchange with the atmospheric neutrals, as a function of the impact parameter p (which defines the ionization point). We consider here the most constraining configuration, for a maximum number of collisions, with 20 keV ENAs/protons and the highest cross-section values available.

[55] Figure 4 shows a step curve, with transitions at each period, since the probability for an ion to collide with neutrals is maximum near the closest point to Titan, which occurs at each gyration period (the ionization point, at $t = 0$, is at a closest point from Titan). Moreover, the steps decrease with the impact parameter, since, the neutral densities are decreasing with altitude: the further from Titan the ENAs get ionized, the more time the new ions need to statistically undergo one collision with the neutrals.

[56] The transition between 0 and 1 period, which corresponds to the impact parameter below which a proton will be neutralized almost instantaneously (before having to complete a gyration), is here around $p = 1680$ km altitude. The particle may even undergo multiple ionizations/neutralizations. This transition depends on the configuration, the ENA energy and the cross-section values considered: it can go down to $p = 1500$ km altitude.

[57] This simple analysis is not enough to estimate precisely the ionization/neutralization transitions which can occur to ENAs, since this gives only statistical results, for simplified configurations (one pitch angle considered, no angular scattering, etc.), but it shows that ENAs ionized can eventually be reneutralized and then be detected by the instrument (with a line of sight which is either the same as the initial one or different). Thus we really need to take into account multiple ionizations/neutralizations to understand the ENA dynamics in the Titan atmosphere.

5. Thermalization of H ENAs

[58] The previous sections showed that energetic particles (protons/H ENAs) may undergo multiple ionizations/neutralizations by charge transfer reactions with the Titan atmospheric neutrals, and we estimated this number of collisions. During these collisions, what energy is lost by the particle? For which altitude do we have a significant thermalization of it?

[59] If we consider a particle coming from the infinity, along a line of sight (for the ENA imager) defined by an impact parameter p, and if we calculate the statistical number of collisions by charge stripping and charge exchange it undergoes (assuming a linear trajectory), we can then infer the energy lost during the crossing of the Titan atmosphere. It will indeed be given by the total number of collisions multiplied by 30 eV, which is the energy loss during a charge transfer collision [*Jasperse and Basu*, 1982] for protons with energies around 1–100 keV.

[60] Such calculations lead to the result shown on Figure 5, which gives the final energy (at the ENA imager

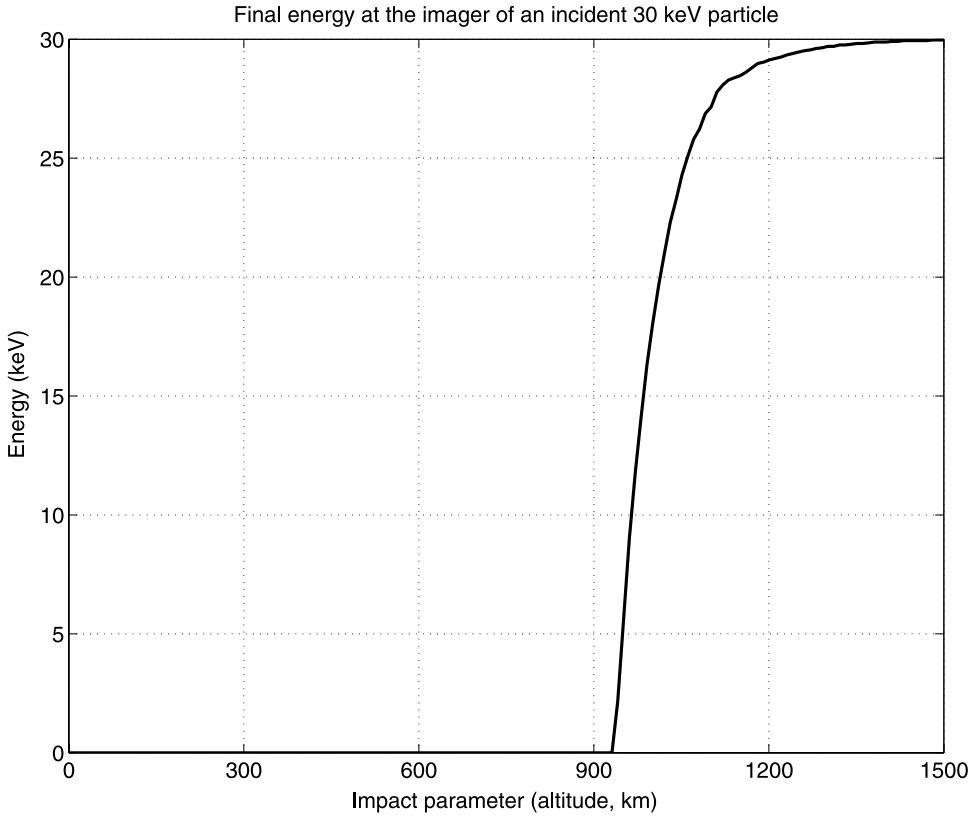

Figure 5. Final energy of an incident 30 keV particle (ion or ENA) when it reaches the imager, after eventually multiple charge transfer collisions (process nos. 1, 2, 3).

positioned at 8000 km altitude) of an initially 30 keV particle, after multiple ionizations/neutralizations in the Titan atmosphere. Below 1000 km altitude, the energy loss becomes substantial, with eventually a full thermalization of the particle, and the ENA imager will not be able to detect them. As a consequence, the emission limit determined by the thermalization only is situated around 1000 km altitude, well below the exobase (H_c = 1425 km). This is consistent with the low altitude INCA observations (i.e., when the orbiter is very close to Titan) during the Titan flybys, and in particular with images where the optical axis of the instrument was perpendicular to the nadir direction: these images show a clear cut-off for the ENA emissions along a horizon line around 1000 km altitude, with high ENA fluxes above this altitude (Mitchell, private communication).

[61] Thus, the ENA emission cut-off altitude should be between 1000 km and 1550 km altitude, depending on whether the thermalization is the only mechanism to take into account for the ENA loss or not. In particular, if a significant part of the energetic particles leaves the Titan atmosphere as ions, these particles will be lost for the ENA imaging, inducing an emission cut-off well above 1000 km altitude.

6. Roelof ENA Exospheric Theory

[62] We have previously shown that multiple ionizations/neutralizations by charge transfer collisions with the atmospheric neutrals have to be taken into account, in order to understand the ENA dynamics: they induce a thermalization for the energetic particles, as well as a change of the charge state which could also play a role. We will now use the analytic formalism on the exospheric emissions developed by Roelof (private communication), which takes into account these mechanisms.

6.1. Formalism

[63] A theory was recently developed (Roelof, private communication) on the ENA emissions from exospheres of planets and moons. This theory is based on a coupled set of transport equations for energetic ions and their emerging ENAs, which is derived in the extreme-forward-scatter approximation on the basis of the generalized Galand-Richmond theorem (that assigns an invariant to ENAs, produced in magnetic fields, similar in form to the well known magnetic moment for energetic ions).

[64] This formalism, which takes into account the multiple charge transfer ionizations/neutralizations, provides in particular very useful analytic expressions for the ENA intensity (assuming a detection point at high altitude). However, we shall separate between three domains: the optically thick part of the atmosphere, the optically thin part with exponentially decreasing neutral profiles and the optically thin part with neutral densities following a $\frac{1}{r^2}$ law (which corresponds to the region dominated by satellite particles).

[65] We can calculate, in the optically thick part of the atmosphere, the ENA flux $J_{ENAthick}$ (cm^{-2} sr^{-1} s^{-1} keV^{-1}) at the energy E, and for an impact parameter p (which

defines the line of sight considered for the instrument), thanks to the knowledge of the isotropic ion flux J_{ION} (with same units as for ENA flux), as a function of the optical thickness τ^c:

$$\frac{J_{ENA_{thick}}(p,E)}{J_{ION}(E)} = \frac{\sigma^{1,0}}{\sigma^c} F(\tau^c) \tag{7}$$

$$F(\tau^c) = e^{-k\tau^c} - e^{-\tau^c} \tag{8}$$

$k \approx \dfrac{W(keV)*\left(\gamma_\sigma + \gamma_j\right)}{E(keV)} \approx \dfrac{90*10^{-3}}{E(keV)}$: the energy E is here about 20–50 keV, W is the energy loss at each charge transfer collision (about 0.03 keV for 1–100 keV protons [see *Jasperse and Basu*, 1982]), and γ_σ/γ_j are the power law coefficients fitting (for a $E^{-\gamma}$ law) the profiles versus energy of respectively the charge transfer cross-sections/parent ions flux [given in *Garnier et al.*, 2007b]; $\sigma^c = \sigma^{0,1} + \sigma^{1,0}$ gives the sum of the ionization $\sigma^{0,1}$ and neutralization $\sigma^{1,0}$ cross-sections (respectively of the ENA and of the corresponding singly charged ion) by charge transfer collision with the neutral species concerned.

[66] The optical thickness τ^c along the line of sight (determined by the impact parameter p) is defined by:

$$\tau^c(p) = \sigma^c \xi(p) = \sigma^c \int_{-\infty}^{+\infty} n(s_p) ds_p \tag{9}$$

with the path column density ξ easily calculated by assuming exponentially decreasing neutral densities n (except in the region dominated by satellite particles).

[67] The ENA flux, in the optically thin parts ($\tau^c \ll 1$) of the atmosphere, is given by:

$$\frac{J_{ENA_{thin}}(p,E)}{J_{ION}(E)} = \sigma^{1,0} \xi(p) \tag{10}$$

with the path thickness being calculated with the assumptions on the neutral profiles, for both optically thin parts of the atmosphere (respectively with exponential and $\dfrac{1}{r^2}$ laws).

[68] We may add that the dominant species below 2000 km altitude, N_2, has a scale height of about H = 80 km at the exobase ($H = \dfrac{kT}{mg}$, with the Boltzmann constant k, the temperature $T \sim 150$ K, the gravitational field g and species mass m). The dominant species at higher altitudes is H_2, with a scale height of 2200 km at the exobase.

6.2. Simulation and Comparison With INCA Measurements

[69] The neutral densities taken, in order to use the formalism discussed above, come from the D. Toublanc atmospheric model (adapted from *Toublanc et al.* [1995]) under the exobase (H_c = 1425 km), combined with a reconstructed exosphere model issued from the *Garnier et al.* [2007] and *Garnier* [2007] model, for the 5 main species at the exobase: N_2, H_2, CH_4, H and $N(4S)$. We modified indeed our model to make it consistent with the Roelof formalism, by adjusting the position of the two limits between the three exosphere domains: the minimization of the errors between this reconstructed model and our exosphere model leads to H_1 = 1550 km (boundary between optically thick and thin exponential atmosphere) and H_2 = 3000 km altitude (boundary between thin exponential atmosphere and $\dfrac{1}{r^2}$ exosphere) for these limits.

[70] The ion flux for energies between 20 and 50 keV have been obtained from the A channels data of the LEMMS instrument, acquired during the Ta Titan flyby (previously shown in *Garnier et al.* [2007a]).

[71] The INCA data acquired during the Ta flyby, and discussed in our previous paper, have now been reprocessed. High spatial resolution single images (not averaged over consecutive image acquisitions) are here used, to minimize any smearing resulting from changing Titan apparent diameter in the INCA field of view due to spacecraft motion, and final ephemeris data for the spacecraft trajectory are used in the projections calculations. This resulted in some adjustments of the spatial representation of objects in the INCA field of view, and the maximum ENA flux appears now closer to Titan (~1000 km closer).

[72] The results of the simulations are shown in Figure 6, for ENA flux integrated over the 20–50 keV energy range. The blue curve shows the calculated flux issued from the Roelof formalism. Even if the theoretical maximum (defined by τ^c(20–50 keV) = 5.2–6.2) is expected around 1350 km altitude, the angular scattering of the ENAs through the instrument entrance foil [*Krimigis et al.*, 2004], modeled here by a gaussian distribution, results in a translation of this maximum toward 1950 km altitude. The red and green curves show respectively the maximum and minimum ENA flux measured during the Ta flyby (by interpolating the reprocessed image of the 26th October 2004, between 15h01 et 15h05). Moreover, we used a two-dimensional numerical model, developed from the model introduced in *Garnier et al.* [2007], by adding the finite gyroradii effects developed in section 2: the resulting profile is shown in dashed black, with a lower limit for the ENA emission placed at 1475 km altitude, near the exobase, and a position of Cassini at 8000 km altitude. We may add that we chose here the INCA measurements in the region where the gyroradii effects have no significant influence (that is to say where we see a bright ENA crescent), to provide a better constraint on the ENA dynamics in the Titan atmosphere.

[73] The comparison between both types of simulations and the measurements indicates a good agreement for the ENA profiles: the maximum ENA flux altitude is exactly reproduced, and the difference in the flux values are very consistent with the uncertainties on the ENA flux measurements (considering uncertainties of at least a factor two).

[74] These simulations, combined with the numerous INCA observations during the Titan flybys indicating a clear maximum ENA flux altitude around 2000 km altitude as during the Ta flyby [*Garnier et al.*, 2007b], allow us to reach this conclusion: the observed Titan ENA halo for high altitude imaging, which is maximum around 2000 km altitude, is related to a lower limit for ENA emission roughly around the exobase (and not around 1000 km altitude, as

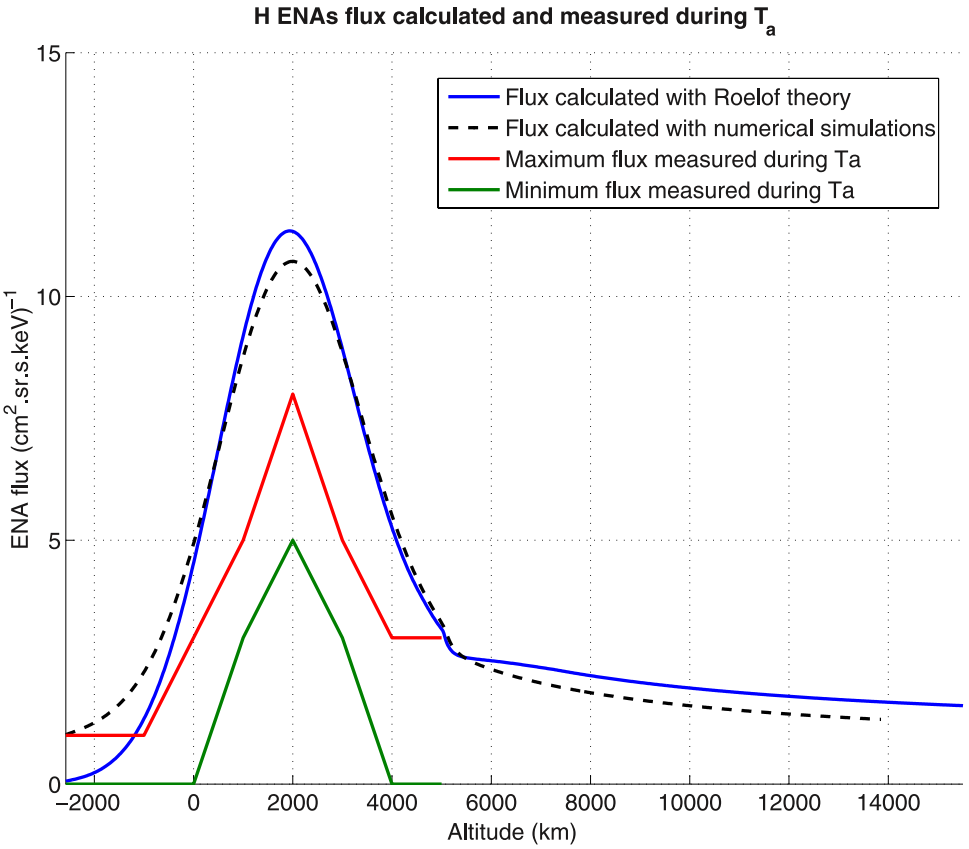

Figure 6. Comparison between the simulations and the measurements for the ENA profiles during the Ta flyby for an altitude of about 8000 km and energies between 20 and 50 keV. We show here the reprocessed INCA data (minimum and maximum in green and red, the simulations with the Roelof formalism (blue) and a two-dimensional numerical model (dashed black). See text for more details.

would imply pure thermalization) before the angular scattering induced by the carbon foil of the instrument.

7. Summary

[75] Following the first Titan flybys we performed a first analysis of the INCA data for the Ta flyby (26 October 2004) in *Garnier et al.* [2007a]. In that paper, we proposed a one-dimensional model for the ENA flux calculation, and a new exosphere model based on the Cassini data.

[76] Our purpose here was to study the ENA absorption mechanisms in the Titan atmosphere, and to determine the lower altitude for the ENA emissions, that can be imaged by remote sensing. We considered the condition for the Ta flyby and an energy range for the H ENAs of 20–50 keV.

[77] First, we studied the finite gyroradii effects which induce a shadow for the parent ions, and thus for the ENA production. Those effects were previously discussed in *Dandouras and Amsif* [1999] for circular trajectories. However, the ion trajectories are rather cycloidal, when taking into account the plasma corotation velocity. We introduced these trajectories and estimated the following finite gyroradii effects, assuming a hard limit for energetic particles at the exobase.

[78] Then, we analyzed the main absorption mechanisms, with the charge stripping on atmospheric neutrals being the most significant, by calculating the optical thickness (which corresponds to the statistical number of collisions) for the ENAs for these collisions. We inferred that ENAs may be ionized up to 1550 km altitude (in impact parameter).

[79] However, the ionized ENAs can be neutralized again, by charge exchange with the atmospheric neutrals. We simulated this mechanism, by estimating the condition for such reneutralizations of ions with cycloidal trajectories: it appears that ENAs once ionized, along a line of sight defined by an impact parameter around 1500–1700 km altitude, can be neutralized again almost instantaneously (or after one or several gyrations for higher impact parameters). As a consequence, we need to take into account multiple ionizations/neutralizations to properly understand the ENAs dynamics.

[80] The main consequence of these multiple ionizations/neutralizations is also the eventual thermalization of the energetic particles. We then calculated the energy lost during the crossing of the atmosphere, which lead to the conclusion that 20–50 keV ENAs are fully thermalized below an impact parameter with 1000 km altitude. This is consistent with the observations of high ENA flux only above 1000 km altitude when Cassini is at low altitudes inside the Titan atmosphere.

[81] The Figure 7 gives a schematic view of the dynamics of ENAs in the Titan atmosphere. First, we consider an

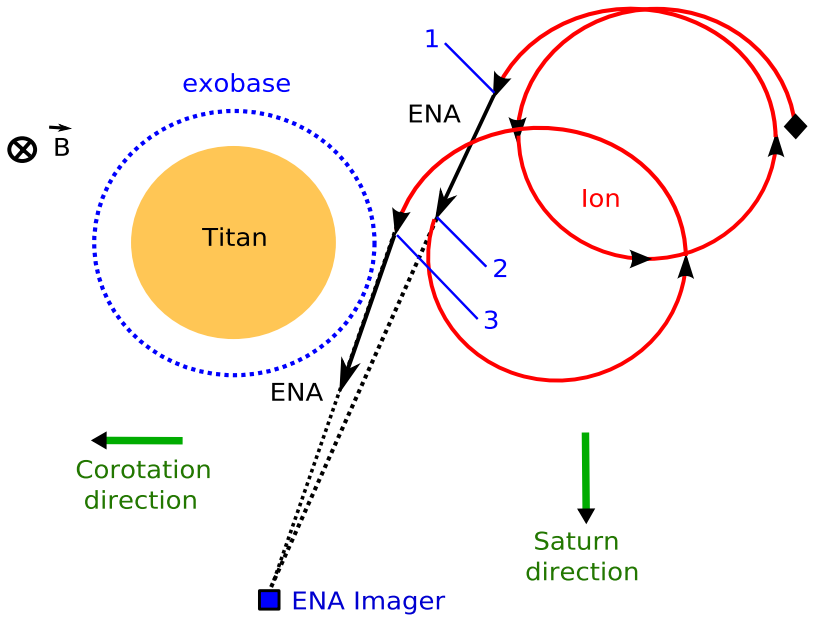

Figure 7. This figure gives a schematic view of the dynamics of an energetic particle in the Titan atmosphere, with the directions of the corotation, Saturn, and the magnetic field indicated. An energetic ion, with a large gyroradius, has a cycloidal motion, is then neutralized (process no. 1 at point 1), the produced ENA is later ionized (process no. 2, at point 2), before the new ion finally leads to an ENA (process no. 3, at point 3) which is detected by the ENA imager. The length scales and the number of collisions used in the figure are chosen for a better understanding.

energetic ion (initial position given by the diamond), which has a cycloidal motion determined by the corotation direction and velocity. Then, at point "1," the ion is neutralized (process no. 1), through a charge exchange collision with atmospheric neutrals, producing an ENA. The ENA may later, at point "2," undergo a charge stripping reaction with neutrals (process no. 2), leading back to an ion charge state. Finally, after eventually a large number of such collisions, a last neutralization (process no. 3) produces an ENA which can be detected by the instrument. However, the particle may also have been thermalized by the collisions or have escaped the Titan's atmosphere as an ion. Moreover, the finite gyroradii effects introduce a large asymmetry in the dynamics of the ENAs.

[82] In the last section we applied the ENA exospheric theory developed recently by Roelof (private communication), which gives analytical expressions for the ENA flux (integrated along the lines of sight of an instrument), and which takes into account the multiple ionizations/neutralizations which can occur to the ENAs/parent ions. The results gave ENA flux profiles very similar to the reprocessed Ta observations, with an ENA peak around 2000 km altitude. Moreover, they were similar to two-dimensional numerical simulations using an ENA emission limit near the exobase (H_c = 1425 km altitude), leading to the same ENA flux altitude after the instrumental angular scattering.

[83] Numerous INCA observations for the first Titan flybys were analyzed [*Garnier et al.*, 2007b], indicating a clear maximum ENA flux altitude ~2000 km altitude as during the Ta flyby (for an imager at high altitude). Combined with our simulations, this implies an ENA emission limit situated around the exobase.

8. Discussion: Complex ENA Dynamics

[84] The proposed analysis converge on such a scenario for the ENA dynamics: the ENAs produced are thermalized, by charge transfer collisions (after multiple ionizations/neutralizations) only around 1000 km altitude, but their ionization, despite of an eventual reneutralization, prevents them from being detected as ENAs, inducing a lower limit for emission roughly around the exobase (~1425 km altitude). However, this scenario assumes that a significant part of the ENAs ionized remain in this charge state, so that they cannot be detected as neutrals by the ENA imager. Otherwise, the ENA emission limit should be closer to the limit related to the thermalization process.

[85] However, the comparison between the charge stripping and charge exchange cross-sections shows values similar or higher for the neutralization mechanism. This would imply that only 25–50% of the energetic particles with trajectories defined by impact parameters between 1000 km and 1500 km altitude (the region where particles undergo multiple ionizations/neutralizations without being fully thermalized), can leave the Titan atmosphere as ions, and not as ENAs.

[86] As a consequence, a doubt remains about our knowledge of the real dynamics of the ENAs in the region between 1000 km altitude and the exobase, which should be detected for most of them, but which are not, by an imager at high altitude. We showed indeed that the ENA

images at high altitudes correspond to a lower limit for ENA emission around the exobase, not around 1000 km altitude.

[87] It should be noted, however, that the numerical simulations, as well as the analytical theory developed by Roelof (private communication), which takes into account the multiple ionizations/neutralizations undergone by the energetic particles, gives results very consistent with the observations for an imager at high altitude.

[88] Other specific mechanisms should be studied in the future, which were not considered here. First, the Coulomb drag induced by collisions with ionospheric particles might play a role on the energetic ions, since the Titan ionosphere is dense. Second, the angular scattering implied by the various collisions (mainly by charge transfer, but perhaps also by Coulomb interactions), and by the gyration motion during the ion charge state, could influence the particles trajectories and thus the ENA imaging. We plan, in our future investigations, to develop a Monte Carlo simulation taking into account the various collisions in the atmosphere, and to combine a hybrid code for the Titan interaction with an ENA imaging simulation.

[89] **Acknowledgments.** We are grateful to Pr. K.C. Hsieh for his great work on the determination of cross-sections for various charge transfer reactions, which was very useful in this study. We would also like to thank Ronan Modolo and Gerard Chanteur for helpful discussions and comments, as well as J. Lilensten and R. Thissen for their precious help on the search for specific reaction cross-sections.

[90] Wolfgang Baumjohann thanks the reviewers for their assistance in evaluating this paper.

References

Amsif, A., J. Dandouras, and E. C. Roelof (1997), Modeling the production and the imaging of energetic neutral atoms from Titan's exosphere, *J. Geophys. Res.*, *102*, 22,169–22,181.

Backes, H., et al. (2005), Titan's magnetic field signature during the first Cassini encounter, *Science*, *308*, 992–995.

Barnett, C. F., and H. K. Reynolds (1958), Charge exchange cross sections of hydrogen particles in gases at high energies, *Phys. Rev.*, *109*(2), 355–359.

Brecht, S. H., J. G. Luhmann, and D. J. Larson (2000), Simulation of the saturnian magnetospheric interaction with Titan, *J. Geophys. Res.*, *105*, 13,119–13,130.

Dandouras, J., and A. Amsif (1999), Production and imaging of energetic neutral atoms from Titan's exosphere: A 3-D model, *Planet. Space Sci.*, *47*, 1355.

Eliot, M. (1977), Sections efficaces d'echange de charge σ_{10} et d'ionisation σ_{01} d'ions et d'atomes d'hydrogene, dans la gamme d'energie de 1 a 20 keV, sur les gaz N_2, CH_4, C_2H_6, C_3H_8 et C_4H_{10}, *J. Phys.*, *38*, 21–27.

Garnier, P., et al. (2007a), The exosphere of Titan and its interaction with the kronian magnetosphere: MIMI observations and modeling, *Planet. Space Sci.*, *55*, 165–173.

Garnier, P., et al. (2007b), Etude de l'interaction entre l'exosphere de Titan et la magnetosphere kronienne, a l'aide des donnees de l'experience MIMI a bord de Cassini, Ph.D. thesis, Universite Paul Sabatier, Toulouse.

Hartle, R. E. (2006a), Initial interpretation of Titan plasma interaction as observed by the Cassini plasma spectrometer: Comparisons with Voyager 1, *Planet. Space Sci.*, *54*, 1211–1224.

Hartle, R. E. (2006b), Preliminary interpretation of Titan plasma interaction as observed by the Cassini Plasma Spectrometer: Comparisons with Voyager 1, *Geophys. Res. Lett.*, *33*, L08201, doi:10.1029/2005GL024817.

Hill, G. (1878), Researches in the lunar theory, *Am. J. Math.*, *1*, 5–26, 129–147, 245–260.

Jasperse, J. R., and B. Basu (1982), Transport theoretic solutions for auroral proton and H atom fluxes and related quantities, *J. Geophys. Res.*, *87*, 811–822.

Kallio, E., I. Sillanpää, and P. Janhunen (2004), Titan in subsonic and supersonic flow, *Geophys. Res. Lett.*, *31*, L15703, doi:10.1029/2004GL020344.

Krimigis, S. M., et al. (1981), Low-energy charged particles in Saturn's magnetosphere: Results from Voyager 1, *Science*, *212*, 225–231.

Krimigis, S. M., J. F. Carbary, E. P. Keath, T. P. Armstrong, L. J. Lanzerotti, and G. Gloeckler (1983), General characteristics of hot plasma and energetic particles in the saturnian magnetosphere: Results from the Voyager spacecraft, *J. Geophys. Res.*, *88*, 8871–8892.

Krimigis, S. M., et al. (2004), Magnetosphere imaging instrument (MIMI) on the Cassini Mission to Saturn/Titan, *Space Sci. Rev.*, *114*, 233–329.

McClure, G. W. (1966), Electron transfer in proton-hydrogen-atom collisions: 2–117 keV, *Phys. Rev.*, *148*, 47–54.

Mitchell, D. G., et al. (2005), Energetic neutral atom emissions from Titan interaction with Saturn's magnetosphere, *Science*, *308*, 989–992.

Neubauer, F. M., et al. (1984) in *Saturn*, edited by T. Gehrels and M. S. Matthews, pp. 760–787, Univ. of Ariz. Press, Tucson.

Neubauer, F. M., et al. (2006), Titan's near magnetotail from magnetic field and electron plasma observations and modeling: Cassini flybys TA, TB, and T3, *J. Geophys. Res.*, *111*, A10220, doi:10.1029/2006JA011676.

Phaneuf, R. A., et al. (1978), Single-electron capture by multiply charged ions of carbon, nitrogen, and oxygen in atomic and molecular hydrogen, *Phys. Rev. A*, *17*, 534–545.

Roelof, E. C. (1987), Energetic neutral atom image of a storm-time ring current, *Geophys. Res. Lett.*, *14*, 652–655.

Rudd, M. E., et al. (1983), Cross sections for ionisation of gases by 5–4000 keV protons and for electron capture by 5–150 keV protons, *Phys. Rev. A*, *28*, 6.

Schunk, R. W., and A. F. Nagy (2000), *Ionospheres: Physics, Plasma Physics, Chemistry*, Cambridge Univ. Press, New York.

Sittler, E. C., Jr., R. E. Hartle, A. F. Viñas, R. E. Johnson, H. T. Smith, and I. Mueller-Wodarg (2005), Titan interaction with Saturn's magnetosphere: Voyager 1 results revisited, *J. Geophys. Res.*, *110*, A09302, doi:10.1029/2004JA010759.

Szego, K., et al. (2005), The global plasma environment of Titan as observed by Cassini Plasma Spectrometer during the first two close encounters with Titan, *Geophys. Res. Lett.*, *32*, L20S05, doi:10.1029/2005GL022646.

Toburen, L. H., et al. (1968), Measurement of high-energy charge-transfer cross sections for incident protons and atomic hydrogen in various gases, *Phys. Rev.*, *171*, 114–122.

Toublanc, D., et al. (1995), Photochemical modeling of Titan's atmosphere, *Icarus*, *113*, 2–26.

Vervack, R. J., et al. (2004), New perspectives on Titan's upper atmosphere from a reanalysis of the Voyager 1 UVS solar occultations, *Icarus*, *170*, 91–112.

Wahlund, J.-E., et al. (2005), Cassini measurements of cold plasma in the ionosphere of Titan, *Science*, *308*, 986–989.

Waite, J. H., et al. (2005), Ion neutral mass spectrometer results from the first flyby of Titan, *Science*, *308*, 982–986.

P. C. Brandt, S. M. Krimigis, D. G. Mitchell, and E. C. Roelof, Applied Physics Laboratory, Johns Hopkins University, Laurel, MD 20723, USA.

I. Dandouras and D. Toublanc, Centre d'Etude Spatiale des Rayonnements, 9 Avenue du Colonel Roche, Toulouse 31028, France.

O. Dutuit, Laboratoire de Planetologie de Grenoble, Universite Joseph Fourier, 38041 Grenoble, France.

P. Garnier and J.-E. Wahlund, Swedish Institute of Space Physics, Uppsala Division, P.O. Box 537, SE-751 21 Uppsala, Sweden. (garnier@irfu.se)

D. C. Hamilton, Department of Physics, University of Maryland, College Park, MD 20742, USA.

N. Krupp, Max-Planck-Institut fur Sonnensystemforschung, Lindau, D-37191, Germany.